Applied Geochemistry 100 (2019) 234–243

Contents lists available at ScienceDirect

Applied Geochemistry

journal homepage: www.elsevier.com/locate/apgeochem

On-line monitoring of the gas composition in the Full-scale Emplacement experiment at Mont Terri (Switzerland)

Yama Tomonaga[a,b,*], Niels Giroud[c], Matthias S. Brennwald[b], Edith Horstmann[b], Nikitas Diomidis[c], Rolf Kipfer[b,d,e], Paul Wersin[a]

[a] Institute of Geological Sciences, University of Bern, Baltzerstrasse 1 + 3, CH-3012, Bern, Switzerland
[b] Eawag, Swiss Federal Institute of Aquatic Science and Technology, Überlandstrasse 133, CH-8600, Dübendorf, Switzerland
[c] Nagra, National Cooperative for the Disposal of Radioactive Waste, Hardstrasse 73, CH-5430, Wettingen, Switzerland
[d] ETH Zurich, Institute of Biogeochemistry and Pollutant Dynamics, CH-8092, Zurich, Switzerland
[e] ETH Zurich, Institute of Geochemistry and Petrology, CH-8092, Zurich, Switzerland

ARTICLE INFO

Keywords:
Gas exchange
Radioactive waste disposal
Opalinus Clay
Bentonite
Pore space

ABSTRACT

An on-line gas monitoring has been conceived and implemented to study the evolution of the composition of the free gas phase in the Full-scale Emplacement (FE) experiment in the Underground Rock Laboratory at Mont Terri (Switzerland). The FE experiment is a trial run for a spent-fuel emplacement drift for a repository according to the Swiss concept for radioactive waste disposal. The monitoring of gas species such as He, Ar, Kr, Xe, N_2, O_2, H_2, CH_4, and CO_2 was performed successfully over several months. The partial pressures of gases relevant for the operational safety such as H_2 and CH_4 have been found to be below the concentration threshold for ignition. The combination of the on-line monitoring data and conventional noble-gas isotope measurements reveals rapid gas exchange between the pore space of the compacted bentonite granulate material used as backfilling and both the access niche and the host rock surrounding the FE tunnel (Opalinus Clay). Such fast gas exchange partly explains the disappearance of oxygen from the bentonite pore space detected by O_2 sensors even prior to sealing of the drift and the accumulation of a fraction of terrigenic gases such as ^{4}He, ^{40}Ar, CH_4, and CO_2.

1. Introduction

The build-up of pressure due to gas generation is an important element in the safety assessment of deep geological repositories for radioactive waste disposal. Different processes are expected to produce or consume gas, which will have a direct influence on the composition of the gas phase and the pressure build-up (Diomidis et al., 2016). The accuracy of the evaluation and prediction of safety-relevant processes can be increased through the quantification of the rates of gas production/consumption and the understanding of the underlying mechanisms. This should help to better address topics such as corrosion and material selection for canisters.

In this context, the Full-scale Emplacement (FE) experiment at the Mont Terri rock laboratory (Switzerland) is a unique opportunity to study the evolution of the gas composition in the near-field of an emplacement drift for spent fuel (SF) according to the Swiss concept for radioactive waste disposal during the early period after closure (see Müller et al., 2017). A simplified sketch of the FE experiment is shown in Fig. 1. The 50-m-long tunnel of the FE experiment has been excavated in the Opalinus Clay (OPA) formation of the Jura mountains. The first 10 m of the tunnel serve as access to a 5-m-thick concrete plug sealing the experiment. The completion of the plug on February 2015 sets the closure time of the FE experiment. Behind the concrete plug, a 23-m-long test section hosts three heaters simulating the thermal behavior of waste canisters containing SF. The deepest part of the tunnel is a 12-m-long interjacent sealing section (ISS) that, according to the Swiss concept for SF disposal (Nagra, 2010), should prevent axial flow paths for radionuclides along the tunnel lining. While all other sections of the tunnel have been covered with shotcrete, the ISS is supported by steel sets only. The test section was backfilled with a compacted granulate bentonite (MX-80), while the ISS was filled partly by porous concrete and by bentonite blocks (for further details see Müller et al., 2017).

Although primarily conceived to investigate repository-induced thermo-hydro-mechanical (THM) coupled effects on the host rock, the FE experiment has been also equipped with gas sensors and gas sampling ports in contact with the pore space of the backfill. In this work, identification and quantification of processes controlling the

* Corresponding author. Institute of Geological Sciences, University of Bern, Baltzerstrasse 1 + 3, CH-3012, Bern, Switzerland.
E-mail address: yama@tomonaga.ch (Y. Tomonaga).

https://doi.org/10.1016/j.apgeochem.2018.11.015
Received 11 December 2017; Received in revised form 19 November 2018; Accepted 19 November 2018
Available online 24 November 2018
0883-2927/

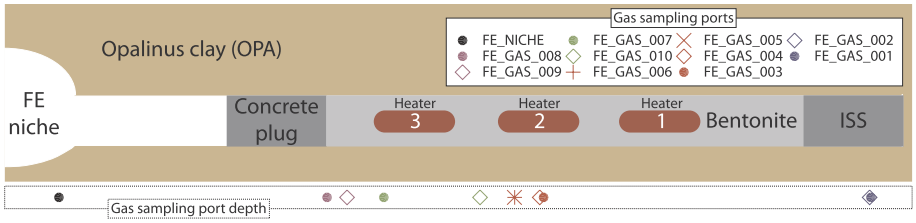

Fig. 1. Simplified sketch of the FE experiment at Mont Terri (St.-Ursanne, Switzerland). The symbols at the bottom of the figure indicate the position along the tunnel where the gas sampling ports are located. ISS: Interjacent sealing section, partly filled with porous concrete.

composition of the gas phase in the near field of the FE experiment have been targeted by the following observational activities: 1) collection of data in the field by on-site monitoring of the gas composition (He, Ar, Kr, Xe, N_2, O_2, H_2, CH_4, and CO_2) in the FE tunnel by means of an on-line mass spectrometer system, 2) regular sampling of the gas phase for precise conventional analyses (e.g., major and trace gases, noble-gas isotopes, alkanes, alkenes, $\delta^{13}C_{CH4}$, $\delta^{2}H_{CH4}$; see also Giroud et al., 2018).

The host rock surrounding the emplacement drift experienced a partial loss of its original water content and is likely characterized by variable permeabilities depending on the drift depth, the radial distance from the drift axis, and the time of the experiment. Accordingly, the effective surface for gas exchange between the gas phase in the drift and the pore water phase in the host rock might vary in space and time. The same applies to the bentonite material used as drift backfill. For instance, fully saturated bentonite is known to have a good sealing ability (Liu et al., 2018a). However, during the initial stages of the FE experiment, the bentonite buffer is far from being saturated and pore water from the host rock is expected to require several years to fill the entire pore space without any external forcing (e.g., water injection; Liu et al., 2018b). Thus, the gas transport properties of the bentonite pore space are likely to change in time.

During the time frame in question, relevant gas transport mechanisms include: diffusion through unsaturated bentonite/OPA, advection through the plug, and exchange with the host-rock pore water. Additionally, experimental artifacts (i.e., specific to the FE experiment as compared with a SF emplacement drift) may also affect the behavior of gases, in particular due to the instrumentation of the experiment.

The present contribution focuses on the on-line monitoring of gas species in the FE experiment and aims to explain the observed phenomena.

2. Materials and methods

The extraction of gases from the bentonite pore space of the FE experiment was performed using a gas circulation system (Gas Module, GM) conceived and built by the company Solexperts AG (Rösli and Lettry, 2016). The on-line monitoring was performed by connecting the inlet of a portable mass spectrometer system (miniRUEDI by Gasometrix GmbH, www.gasometrix.com; Brennwald et al., 2016) to the loop of the GM. Samples for regular gas analysis have been acquired by extending the GM circulation loop with sampling containers connected in series (Swagelok bottles or copper tubes). An overview of the GM and on-line monitoring systems is given in Fig. 2. Details on the gas sampling ports are given in Table 1.

The data presented here were collected between January and July 2017. On the one hand, our measurements do not comprehend the most dynamic phase with regard to THM conditions (Müller et al., 2017) and gas exchange (Giroud et al., 2018) right after the closure of the FE experiment in February 2015. On the other hand, seven months of gas analyses are a rather short period compared to total runtime of the experiment foreseen to last for at least 10–15 more years. Therefore, our investigations have been conducted under conditions that can be considered more or less stable. For instance, changes in temperature inside the experiment are minor (i.e., less than 0.1 °C/month at the middle heater) compared to the preceding two years (more than 2 °C/month).

2.1. Gas circulation system

In total ten gas sampling ports were installed in the FE gallery (Fig. 1; see also Table 1). Seven of these ports are mounted at the tunnel wall. These sampling ports consist of a silver-coated nylon filter hosted on a polyvinylidene difluoride (PVDF) housing. Three sampling ports (FE_GAS_005, FE_GAS_006, and FE_GAS_007) are installed close to the heaters and are designed to withstand higher temperatures (up to 80 °C). Therefore, these sampling ports are equipped with stainless steel filter meshes supported by a PVDF housing.

For gas circulation, each gas sampling port in the FE tunnel is connected with two polyether ether ketone (PEEK) lines (i.e., an inlet and an outlet) to the GM. The two sampling ports FE_GAS_001 and FE_GAS_002 are connected by PEEK lines with an outer diameter of 1/4". All other sampling ports are equipped with 1/8" PEEK lines. The presence of two lines allows mixing and homogenization of the gas phase in the volume comprising the sampling port, the PEEK tubes, and the GM (a total of about 900–1100 mL) at a flow rate of 20 mL per minute. The gases are forced by a membrane pump (KNF N022) from the sampling ports to the GM in one PEEK line and from the GM towards the sampling ports in the second PEEK line. The ten sampling ports are connected to the two automatic VICI® valves of the GM (Fig. 2). In addition, the gas circuit design makes it possible to connect the GM to 1) a closed stainless steel loop (for periods of inactivity or leak testing of the GM), 2) a gas bottle delivering N_2 at atmospheric pressure (about 1 bar) for flushing the GM, and 3) a vacuum pump (KNF N813.4ANE) to evacuate the GM. Before connecting the gas sampling ports to the GM, the latter is pumped (3 min) and flushed with N_2 (3 s) for three times and subsequently evacuated for 20 min until the pressure in the system reaches approximately 0.05 mbar. For the on-line gas monitoring and for the acquisition of gas samples for regular analysis each gas sampling port is connected to the gas circulation system for about 4 h to minimize artifacts resulting from the presence of residual gas with a slightly different composition in the PEEK lines and in the GM. A water trap (SMC AMJ3000-F03) installed on the GM loop upfront the connection to the on-line gas monitoring system prevents the circulation of macroscopic water droplets.

2.2. On-line gas monitoring system

The mass spectrometer system used to monitor gas species in the FE experiment (miniRUEDI, Gasometrix GmbH, Switzerland) is described in detail in Brennwald et al. (2016). The system was originally conceived to allow quantification of the partial pressures of He, Ar, Kr, N_2, O_2, CO_2, and CH_4 in gaseous and aqueous matrices with an analytical uncertainty of 1–3%. In the present work we extended the gas analysis to Xe and H_2. The gas is sampled through a capillary pressure reduction system into a vacuum chamber, where its composition is analyzed in dynamic mode using a quadrupole mass spectrometer (Stanford Research Systems RGA-200).

Calibration of the system is achieved using gas calibration bags (Linde, Plastigas) at an ambient pressure of approximately 960 mbar (see Brennwald et al., 2016). In the analytical setup at Mont Terri two calibration bags are installed. The first bag (AIR) is filled with atmospheric air (for its composition please refer to e.g. Ozima and Podosek, 1983) to calibrate the partial pressures of He, Ar, Kr, Xe, N_2, and O_2.

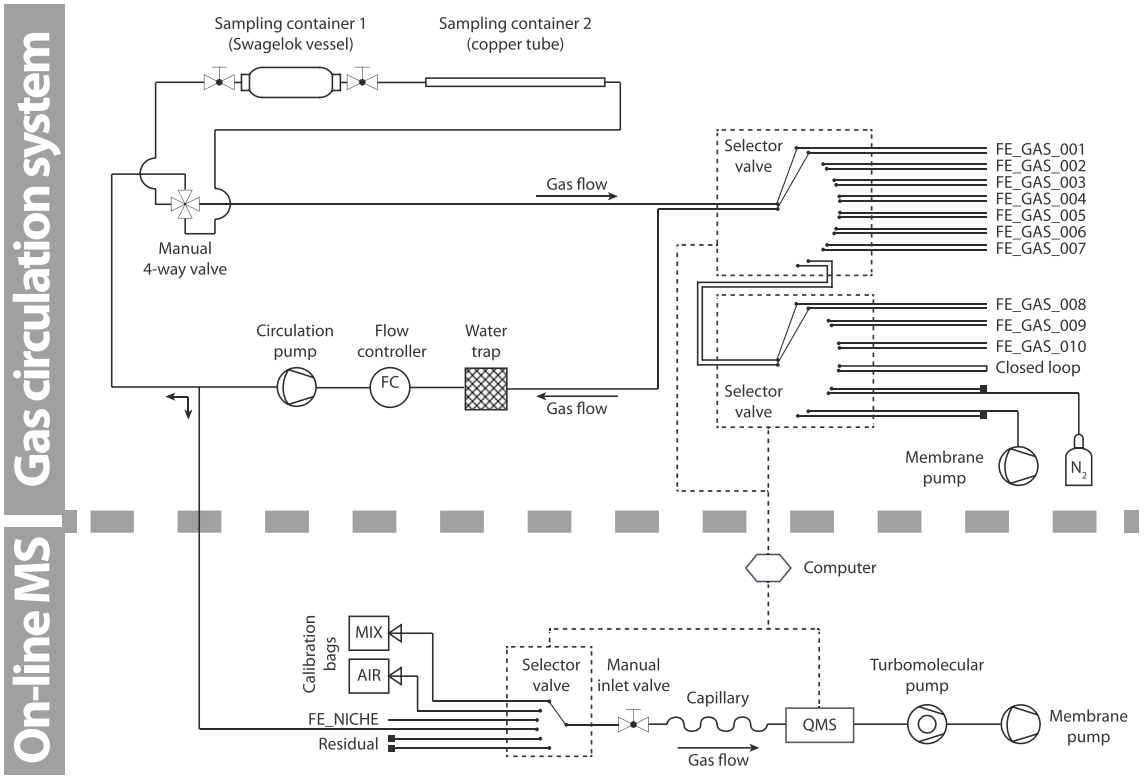

Fig. 2. Schematic overview of gas circulation system and the on-line mass spectrometer installed at the FE experiment. QMS: quadrupole mass spectrometer.

The second bag (MIX) is filled with a gas mixture comprising N_2 (97%), H_2 (1%), CH_4 (1%), and CO_2 (1%).

The capillary inlet of the on-line gas monitoring system is connected to the outlet of a six port selection valve (VICI® C5-2306EMHY, as described in Brennwald et al., 2016). The inlets of the valve were connected to 1) the circulation loop of the GM, 2) the AIR bag, 3) the MIX bag, 4) the atmosphere of the FE niche, 5) a short crimped capillary section for blank determination.

H_2 (m/z = 2), CH_4 (m/z = 15, i.e. the CH_3^+ fragment ion), N_2 (m/z = 28), O_2 (m/z = 32), Ar (m/z = 40), and CO_2 (m/z = 44) are measured on the Faraday cup of the mass spectrometer (where m/z is the mass/charge ratio used for the mass spectrometer analysis). He (m/z = 4), Kr (m/z = 84), and Xe (m/z = 129) are measured on the electron multiplier detector. Each measurement on the Faraday cup consists of 20 reading cycles while for the electron multiplier detector the number of cycles is set to 40. The output of each measurement step consists of the mean intensity for each gas species.

The main loop of the analytical protocol starts with two calibration steps (AIR and MIX) followed by the determination of the analytical blank. Subsequently, gas from the FE niche and from all ten gas sampling ports is analyzed. Instrumental drifts are controlled and corrected by the analysis of gas from both the AIR and MIX calibration bags prior to the measurements of the gas from each sampling port.

The measurements were conducted at the highest frequency (1 measurement every ~4 h). Including the time required for calibration of the system and the analysis of the gas composition in the FE niche, each gas sampling port is measured approximately every 3 days. Leak tests of the GM were conducted before the different measurement blocks (i.e., before starting the monitoring and before resuming it after the computer system malfunction). To this end, the GM was evacuated and afterwards set in closed-loop mode. The on-line mass spectrometer measured the residual gas in the GM over several days. No significant increases in the gas partial pressures have been observed. O_2 contamination was investigated in detail, as any injection of atmospheric O_2 from the FE niche into an O_2-free sampling port would have compromised the validity of the gas monitoring. The maximum leak rate

Table 1
Specifications of the gas sampling ports according to Rösli and Gisiger (2016). The temperature (T) and relative humidity (RH) given in the last two columns have been measured by sensors in the vicinity of the respective sampling port on Jan. 18th, 2017 which coincides with the date of sampling for conventional gas analyses. PL: PEEK line.

Sampling port	Gallery meters [m]	PL diameter ["]	Filter mesh	T [°C]	RH [%]
FE_NICHE	~0	n.a.	Capillary inlet	18.5	47
FE_GAS_001	48.0	1/4	Ag-coated nylon	18.6	45
FE_GAS_002	47.8	1/4	Ag-coated nylon	18.6	44
FE_GAS_003	28.4	1/8	Ag-coated nylon	52.0	89
FE_GAS_004	27.9	1/8	Ag-coated nylon	72.0	64
FE_GAS_005	25.5	1/8	Stainless steel	70.3	52
FE_GAS_006	25.5	1/8	Stainless steel	70.3	52
FE_GAS_007	17.9	1/8	Stainless steel	69.6	45
FE_GAS_008	15.1	1/8	Ag-coated nylon	25.6	50
FE_GAS_009	16.4	1/8	Ag-coated nylon	32.3	57
FE_GAS_010	24.4	1/8	Ag-coated nylon	43.2	48

determined for O_2 was less than 0.7 mbar/day (i.e., a maximum theoretical increase of 0.1 mbar during gas circulation at each sampling port over 4 h) which can be considered negligible with respect 1) to the overall effect on other gas partial pressures, 2) to the analytical precision of the on-line measurements (approximately ± 3 mbar for O_2), and 3) to other atmospheric gas contamination sources (e.g., dead volume of the VICI® valves of the GM, the residual gas in the GM after evacuation).

2.3. Regular gas sampling and analyses

Samples for off-site laboratory-based gas analyses are collected in 75 mL stainless-steel cylinders (Swagelok 304L-HDF4-75-T) closed at both ends with bellows-sealed valves (Swagelok SS-6H-MM connected with SS-6-MTA-1-4 fittings) and in copper tubes sealed airtight with two metal clamps (e.g. Beyerle et al., 2000; Brennwald et al., 2013; Tomonaga et al., 2011; Tyroller et al., 2016). The sampling containers are connected in series to the circulation loop of the GM via a manual four-way Swagelok valve. This valve allows connection of the additional short loop consisting of the sampling containers or bypass of the latter during the on-line monitoring using the mass spectrometer system described in Section 2.2.

The gas samples for noble-gas analysis were collected from a selection of sampling ports adequate to reveal spatial heterogeneities with regards to the noble-gas concentrations in terms of depth within the FE tunnel. Although the gas samples have been acquired three months before the on-site monitoring time period, the results are expected to be comparable, as no major changes are expected in terms of gas exchange dynamics or physical conditions within the FE drift.

The noble gas isotope composition in the collected gas samples was analyzed in the Noble Gas Laboratory at the Swiss Federal Institute of Science and Technology in Zurich (ETH Zurich). Gas aliquots (0.20–0.22 cm^3_{STP}) from each sample were analyzed by static mass spectrometry (Beyerle et al., 2000). After transferring an aliquot into the gas purification system, the gas was separated into a He-Ne fraction and an Ar-Kr-Xe fraction in the purification system using a series of cold traps cooled by liquid nitrogen. A first split of the He-Ne fraction was used for combined analysis of ^{4}He, ^{20}Ne, and ^{22}Ne using a non-commercial sector-field mass spectrometer equipped with a Baur-Signer ion source (Baur, 1980). After He-Ne analysis, the Ar-Kr-Xe fraction was used for combined analysis of ^{36}Ar, ^{40}Ar, ^{86}Kr, and ^{136}Xe using the same mass spectrometer. A second split of the He-Ne fraction was further purified using a cryogenic trap at 70 K and subsequently used for ^{3}He/^{4}He analysis in a Micromass 5400 sector-field mass spectrometer equipped with a Nier-type ion source. Mass spectrometer results were calibrated using aliquots of an air standard collected in Zurich (Switzerland), which were processed exactly in the same way as the sample aliquots. Typical precisions for the concentration measurements are 0.3% (He), 0.9% (Ne), 0.3% (Ar), 0.8% (Kr), and 1.0% (Xe). For the isotope ratios, typical precisions are 0.7% (^{3}He/^{4}He), 0.3% (^{20}Ne/^{22}Ne), and 0.2% (^{36}Ar/^{40}Ar). For further details on the analytical setup used at ETH Zurich please refer to Beyerle et al. (2000).

3. Results and discussion

3.1. On-line gas monitoring

Figs. 3 and 4 summarize the results of the on-line monitoring of the FE experiment at Mont Terri over a time span of about three months. Unfortunately, a computer system malfunction resulted in an apparent data gap for the months of May and June 2017.

The distribution of the O_2 partial pressures is in agreement with the sensor data reported by Giroud et al. (2018) showing that, even prior to closure, a rapid decrease of the O_2 concentrations in the pore space occurred within a few months. Our monitoring data indicate that traces of O_2 (10–40 mbar) are detectable only between the concrete plug and heater 3 in a short tunnel segment being the closest to the FE niche where atmospheric O_2 partial pressures prevail (i.e., about 210 mbar; see Figs. 1, 3 and 4). In the remaining part of the FE tunnel O_2 is virtually absent.

The N_2 partial pressure at each sampling port is inversely correlated to those of O_2 (i.e., the second most abundant gas species; see Figs. 3 and 4). As N_2 is the major gas phase in atmospheric air (Ozima and Podosek, 1983) and in the OPA pore water (Vinsot et al., 2017a), its partial pressures cannot be used to gain additional insights on the gas dynamics in the FE experiment (i.e., very minor changes are likely to occur within the analytical error range). Nevertheless, the N_2 partial pressures reflect the evolution of the total pressure in the system. According to the measured data, the pressure in the bentonite pore space is close to the ambient pressure in the FE niche.

The presence of O_2 in the bentonite pore space immediately behind the concrete plug suggests that the sealing is not fully airtight and air from the FE niche is able to enter the experiment (see Giroud et al., 2018). The existence of a connection between the FE niche and the FE tunnel suggests that the disappearance of O_2 from the bentonite pore space in the early stages of the experiment produced a total pressure drop resulting in a gas flow from the FE niche into the drift. This explains why in general the partial pressures of all atmospheric gases (with the exception of O_2) are higher compared to the respective partial pressures in atmospheric air but the total pressures do not differ significantly from the one in the FE niche. These findings are in line with the interpretation of the spatial distribution of ^{4}He, ^{40}Ar, and CH_4 (see below).

The noble-gas isotopes ^{4}He, ^{40}Ar, and ^{84}Kr in the FE experiment (Fig. 3, colored symbols) are clearly enriched with respect to the air in the FE niche (Fig. 3, black dots), which is close to atmospheric air composition. The partial pressures of ^{4}He and ^{40}Ar increase consistently with increasing tunnel depth (Fig. 4) indicating accumulation of a terrigenic-gas component coupled with transport towards the concrete plug. The migration of ^{4}He (produced from the decay of U and Th in mineral phases; e.g. Mamyrin and Tolstikhin, 1984; Tomonaga et al., 2017) from the OPA pore water into the bentonite pore space is expected. The same applies for radiogenic ^{40}Ar produced from the decay of ^{40}K. Indeed, ^{4}He and ^{40}Ar have been reported to be (highly) enriched in the OPA pore water (e.g., Pearson et al., 2003).

The interpretation of the progressive enrichment of ^{84}Kr with increasing distance from the FE niche (Fig. 4) is less straightforward in terms of terrigenic fluid origin. All gas sampling ports in the bentonite pore space show higher ^{84}Kr partial pressures compared to the FE niche which is charaterized by a ^{84}Kr partial pressure close to the one of atmospheric air (about $6{\cdot}10^{-4}$ mbar).

Previous studies report Kr concentrations in OPA pore water at Mont Terri between air-saturated water (ASW; $(0.8\text{-}1.1){\cdot}10^{-7}$ cm^3_{STP}/g assuming a temperature of 4 °C and a rather reasonable salinity range of 0–35 g/kg; Rübel et al., 2002) and two times AWS (up to $2.1{\cdot}10^{-7}$ cm^3_{STP}/g; Maineult et al., 2013). Furthermore, the dissolved-gas concentrations in the OPA pore water may vary depending on the sampling location within the laboratory at Mont Terri (Pearson et al., 2003) and, hence, a direct comparison with previous studies is not necessarily meaningful. Nevertheless, the observed ^{84}Kr enrichment might be also the result of the gas partitioning between OPA pore water and the free gas phase in bentonite pore space, as discussed in detail in Section 3.2. From this point of view, the decreasing ^{4}He, ^{40}Ar, and ^{84}Kr partial pressures close to the plug indicate that gas exchange between the FE niche and the bentonite pore space occurs.

The ^{129}Xe data series reveals higher partial pressures for this gas species between heater 3 and heater 2 (Fig. 4). Under common environmental conditions (and in absence of a gas purification line) Xe isotopes should be hardly detectable by the adopted mass spectrometer system. However, in the case of the FE experiment the heaters used to mimic the thermal behavior of canisters containing SF had been filled with Xe-spiked N_2 (i.e., 2000 ppmv Xe). Such Xe concentration

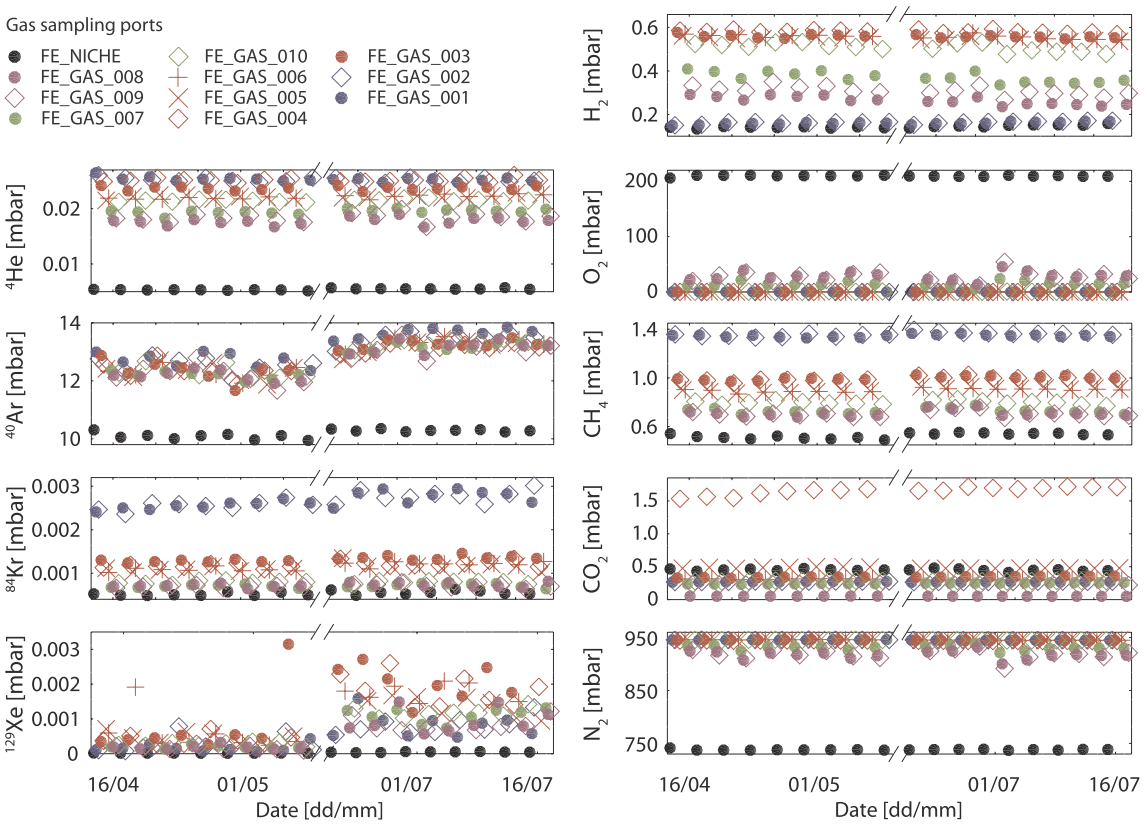

Fig. 3. Gas partial pressures determined during the on-line monitoring of the FE experiment at Mont Terri. Different symbols indicate different sampling ports within the FE tunnel, as shown in Fig. 1.

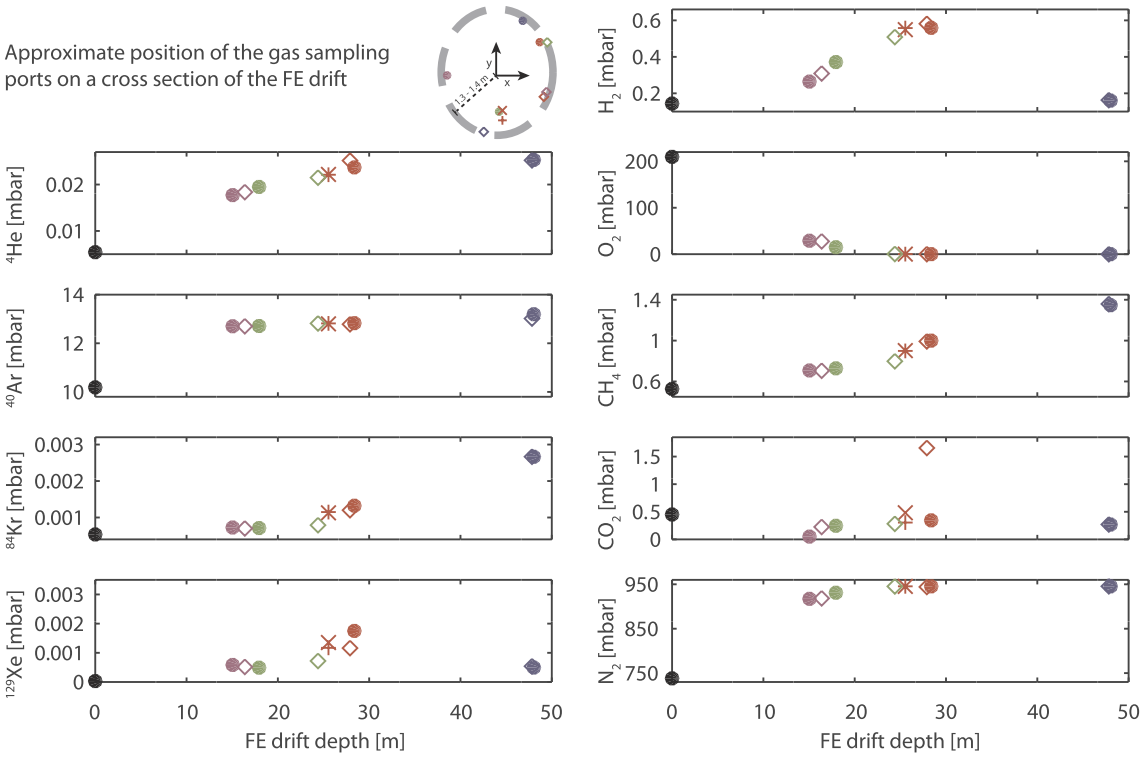

Fig. 4. Gas sampling port depths (abscissa axis, in gallery meters) plotted against the respective average gas partial pressures (ordinate axis) determined during the on-line monitoring of the FE experiment at Mont Terri. The different symbols have the same meaning as in Fig. 1.

Table 2
Noble-gas concentrations and isotope ratios measured in the gas samples collected from the FE experiment at Mont Terri on Jan. 18th, 2017. The noble-gas concentrations and isotope ratios for atmospheric air are reported at the bottom of the table. *A*: gas amount in aliquot. STP = standard temperature (0 °C) and pressure (1 atm).

Sample	*A* [cm^3_{STP}]	He [10^{-5} v/v]	$^3He/^4He$ [10^{-7}]	Ne [10^{-5} v/v]	$^{20}Ne/^{22}Ne$ [-]	Ar [10^{-2} v/v]	$^{36}Ar/^{40}Ar$ [10^{-3}]	Kr [10^{-6} v/v]	Xe [10^{-5} v/v]
FE_GAS_001	0.209	2.71 ± 0.01	4.15 ± 0.07	2.17 ± 0.02	9.77 ± 0.01	1.183 ± 0.001	3.36 ± 0.02	1.49 ± 0.01	1.73 ± 0.01
FE_GAS_002	0.204	2.74 ± 0.01	4.67 ± 0.06	2.18 ± 0.02	9.79 ± 0.01	1.187 ± 0.001	3.365 ± 0.002	1.52 ± 0.01	1.74 ± 0.01
FE_GAS_003	0.217	2.52 ± 0.01	4.70 ± 0.07	2.25 ± 0.02	9.80 ± 0.01	1.177 ± 0.001	3.36 ± 0.01	1.47 ± 0.01	3.66 ± 0.03
FE_GAS_004	0.200	2.62 ± 0.01	5.19 ± 0.08	2.25 ± 0.02	9.81 ± 0.01	1.163 ± 0.001	3.391 ± 0.002	1.43 ± 0.01	3.53 ± 0.03
FE_GAS_009	0.206	1.79 ± 0.01	4.87 ± 0.08	2.12 ± 0.02	9.81 ± 0.01	1.122 ± 0.001	3.40 ± 0.02	1.40 ± 0.01	2.29 ± 0.02
FE_GAS_010	0.209	2.17 ± 0.01	5.03 ± 0.08	2.22 ± 0.02	9.80 ± 0.01	1.179 ± 0.001	3.37 ± 0.01	1.45 ± 0.01	3.83 ± 0.03
Atmospheric air[a]		0.524 ± 0.005	13.9 ± 0.1	1.818 ± 0.004	9.80 ± 0.08	0.934 ± 0.001	3.349 ± 0.003[b]	1.14 ± 0.01	0.0087 ± 0.001

[a] From Ozima and Podosek (1983).
[b] From Lee et al. (2006).

(equivalent to 0.002 mbar) matches rather well the observed Xe partial pressure range between heater 3 and heater 2 (0.001–0.002 mbar; see Fig. 4). It should be noted that the large error of the ^{129}Xe measurements (slightly more than 30%) does not allow identification of a well-defined concentration maximum in terms of FE drift depth. According to a Mont Terri Project report (Aitemin, 2015) heater 3 had a fall incident during the emplacement phase where some cables and fittings connected to the heater body were damaged. In the light of the on-line Xe measurements it seems reasonable to hypothesize that this incident resulted in a minor gas leakage with direct consequences for the overall Xe budget in the bentonite pore space of the FE experiment.

The measurements conducted with the on-line mass spectrometer system reveal that the highest H_2 partial pressures (about 0.6 mbar or 0.06%) can be found close to the central heater (i.e., heater 2; Figs. 1 and 4). It should be noted that the average error of the H_2 measurements (about 0.2 mbar) is large compared to the determined partial pressures. The H_2 spatial distribution (Fig. 4) suggests ongoing anaerobic corrosion of the surface of the heaters or of other metal parts belonging to the instrumentation of the FE experiment being mainly installed at the depth range of the three heaters. Sampling ports FE_GAS_001 and FE_GAS_002 are located in porous concrete characterized by higher pH and, therefore, lower corrosion rates are expected for steel. The agreement of the H_2 partial pressures of FE niche and the deepest part of the FE tunnel (see Fig. 4) indicate that no significant share of H_2 is provided by the OPA.

Methane accumulation occurs concomitant to the migration of other terrigenic gas species. Emanation of CH_4 from the OPA (up to a few % over a time span of less than three years) has been illustrated by a recent study that estimated the pore water concentrations to be about 0.3 mmol/L (Vinsot et al., 2017a). The highest CH_4 concentration determined in the present study (about 1.4 mbar or 0.1% accumulated over approximately two and a half years since experiment closure at ports FE_GAS_001 and FE_GAS_002) agrees with previous observations (Vinsot et al., 2017a) suggesting that the OPA pore water can act as a CH_4 reservoir. Indeed, the CH_4 flux estimated for the FE experiment using the OPA geometric surface (280 m^2) and the bentonite pore space volume (~70 m^3) is about $7{\cdot}10^{-3}$ mol/m^2/yr which roughly agrees with the flux determined in the BHT-1 experiment at Mont Terri (approximately $5{\cdot}10^{-3}$ mol/m^2/yr; Vinsot et al., 2017a). The CH_4 spatial distribution pattern being similar to the one of inert gases such as ^4He and ^{40}Ar (i.e., increasing partial pressures with increasing tunnel depth) indicates that similar transport processes foster the accumulation (and loss) of CH_4 in the bentonite pore space.

At first sight, the measured carbon dioxide partial pressures are similar to the one of atmospheric air (about 0.3 mbar or ~0.03%) with the exception of sampling port FE_GAS_004 being characterized by almost four times higher partial pressures. A small enrichment, enough to be significant with respect to the average analytical error of ± 0.02 mbar, is also observed at sampling port FE_GAS_005. CO_2 partial pressures in the OPA pore water are in the range of 10^{-2} to 10^{-3} bar (e.g., Pearson et al., 2003, 2011; Vinsot et al., 2014). The occurrence of higher CO_2 partial pressures at some sampling ports could indicate microbial activity. As discussed in Section 3.2, the observed CO_2 enrichment may be produced also by the presence of pathways for fluid transport from a different geochemical reservoir towards the bentonite pore space. Such pathways could be related to the extent and geometry of the excavation damaged zone (EDZ) which is about 1–2 times the tunnel radius and is characterized by much higher permeabilities compared to the undisturbed OPA (a few orders of magnitude higher permeabilities within the inner 1 m zone; Bossart et al., 2002). Alternatively, CO_2 originating from the OPA pore water might be consumed at different rates in the vicinity of the respective sampling ports (e.g., by sorption; Giroud et al., 2018). Gas sampling port FE_GAS_008 (located immediately after the concrete plug) is characterized by CO_2 partial pressures being lower (i.e., ~0.05 mbar) than those of the FE niche and of atmospheric air. These lower partial pressures suggest ongoing carbonatation of the concrete plug (possibly also occurring in the porous concrete of the ISS). Nevertheless, other processes could explain the observed lower CO_2 concentrations (see e.g., Vinsot et al., 2017a).

3.2. Off-site laboratory-based analyses

The results of the conventional noble-gas analyses are reported in Table 2.

The measured He, Ar, and Kr concentrations are in general agreement with the measurements of the on-line mass spectrometer system presented in Section 3.1. Similar concentration gradients with respect to the tunnel depth are found for all the gas species. He concentrations are up to five times higher ($2.7{\cdot}10^{-5}$ v/v) than in atmospheric air ($5.2{\cdot}10^{-6}$ v/v). The Ne concentrations, similarly to the other noble gases, are enriched (up to $2.3{\cdot}10^{-5}$ v/v, i.e. an enrichment of 24%) with respect to atmospheric air ($1.8{\cdot}10^{-5}$ v/v). Part of such enrichment could be attributed to the gas flow from the FE niche into the bentonite pore space produced by the disappearance of O_2 (see Section 3.1). Indeed, the induced relative change of the partial pressures is expected to be similar for all atmospheric gases. For instance, the increase of the partial pressure of N_2 is about 20% resulting in an enrichment of approximately 25% compared to the atmospheric N_2 concentration. Nevertheless, Maineult et al. (2013) report Ne pore water concentrations being significantly higher (up to $4.9{\cdot}10^{-7}$ cm^3_{STP}/g and an average of $2.3{\cdot}10^{-7}$ cm^3_{STP}/g) than ASW concentrations ($(1.6\text{-}2.1){\cdot}10^{-7}$ cm^3_{STP}/g assuming a temperature of 4 °C and a salinity range of 0–35 g/kg). Hence, gas originating from the OPA can also contribute to the measured concentrations. The same applies to Ar and Kr showing maximum excesses of 27% and 33%, respectively. Although Pearson et al. (2003) did not find Ne excesses in OPA pore waters, in the same work they report a few Kr (up to $1.3{\cdot}10^{-7}$ cm^3_{STP}/g) and Xe (up to $2.7{\cdot}10^{-8}$ cm^3_{STP}/g) concentrations being slightly higher than ASW ($(0.8\text{-}1.1){\cdot}10^{-7}$ cm^3_{STP}/g for Kr and $(1.2\text{-}1.6){\cdot}10^{-8}$ cm^3_{STP}/g for Xe taking into account the same temperature and salinity conditions used

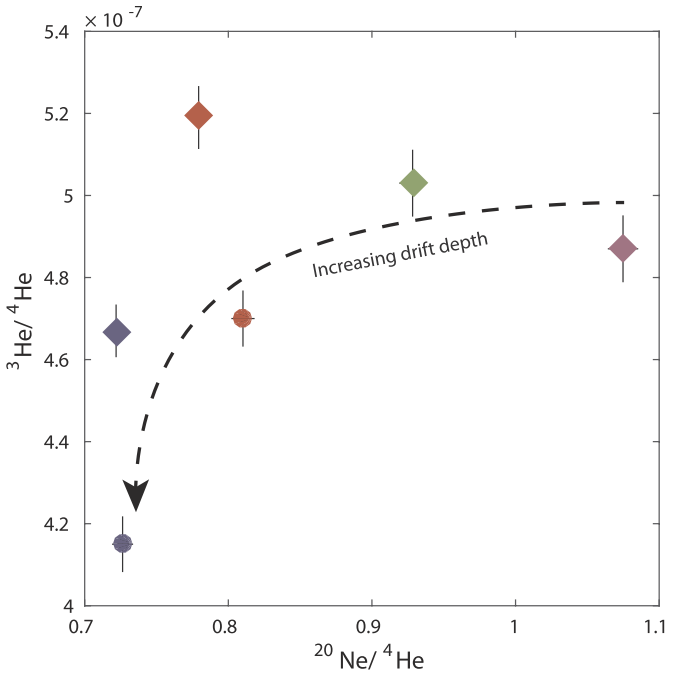

Fig. 5. Three-isotope plot of the $^{20}Ne/^{4}He$ ratios against the $^{3}He/^{4}He$ ratios. The dashed arrow is a visual help to follow the trend in isotope composition changes with the increasing drift depth. Symbol shapes and colors indicate different gas sampling ports as in Fig. 3. The decreasing $^{3}He/^{4}He$ isotope ratios with increasing tunnel depth clearly indicate accumulation of radiogenic ^{4}He from the OPA. A slightly higher $^{3}He/^{4}He$ ratio for a gas sample from a sampling port FE_GAS_004 located in the region of heater 2 might correlate with a CO_2 anomaly detected by the on-line gas monitoring (Section 3.1). (For interpretation of the references to color in this figure legend, the reader is referred to the Web version of this article.)

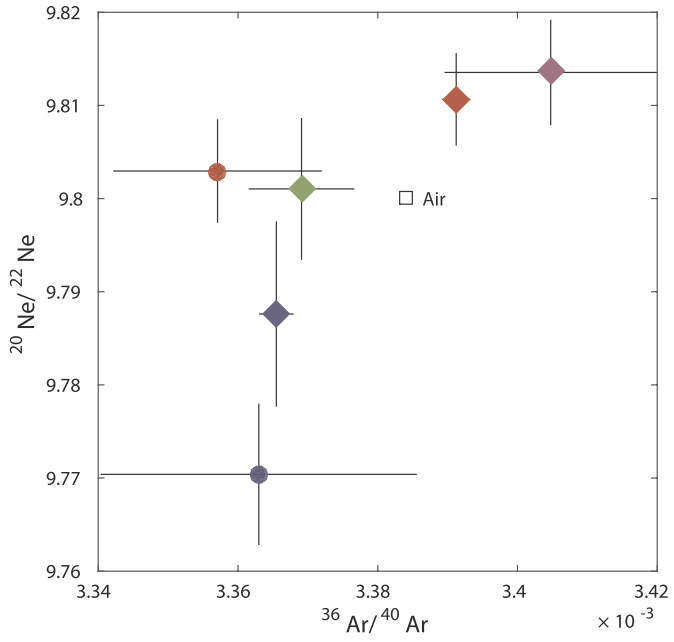

Fig. 6. $^{36}Ar/^{40}Ar$ ratios against $^{20}Ne/^{22}Ne$ ratios. Symbol shapes and colors indicate different gas sampling ports as in Fig. 3. The isotope signature of atmospheric air (e.g. Ozima and Podosek, 1983; Sano et al., 2013) is marked by the open square. Similarly to Fig. 5, there is a trend towards a terrigenic component of the Ar isotopes being enriched in ^{40}Ar. Ne isotope ratios being even higher than the value for atmospheric air might indicate the occurrence of a fractionation process. Although at the moment we cannot fully explain the observed Ne isotope fractionation, it is significant. (For interpretation of the references to color in this figure legend, the reader is referred to the Web version of this article.)

for ASW Ne concentrations). From the previous observations and from our noble-gas measurements it is reasonable to assume that the elemental signature of OPA pore water differs to a certain extent from the one of ASW.

In the three-isotope plot of Fig. 5 the decrease of the values of both the $^{20}Ne/^{4}He$ ratios and the $^{3}He/^{4}He$ ratios with increasing tunnel depth (see Fig. 1 for the position of the sampling ports) indicates accumulation of isotopically heavy He. The terrigenic He source should certainly be the OPA pore water being characterized by a $^{3}He/^{4}He$ ratio with an average of $1.3{\cdot}10^{-7}$ (Pearson et al., 2003; Rübel et al., 2002) or a range of $(1.4–9.1){\cdot}10^{-7}$ (Waber and Rufer, 2017). The higher $^{3}He/^{4}He$ ratio of sample FE_GAS_004 may correlate with the anomalously high CO_2 partial pressures detected by the on-line gas monitoring (Section 3.1) and might suggest the presence of a connection to a geochemical reservoir providing a minor share of fluids slightly enriched in ^{3}He and CO_2. OPA pore waters have been shown to host three to four orders of magnitude higher He concentrations (i.e., from (4–9) $\cdot10^{-5}$ cm^3_{STP}/g up to about $1{\cdot}10^{-4}$ cm^3_{STP}/g; Waber and Rufer, 2017; Pearson et al., 2003; Mazurek et al., 2011) compared to ASW (about $4{\cdot}10^{-8}$ cm^3_{STP}/g; e.g., Kipfer et al., 2002). All evidence indicates that He from the OPA pore water is expected to degas into the bentonite pore space. Assuming that the He isotope ratios in the bentonite pore space result from the binary mixing of atmospheric air and gases from the OPA pore water, the shares of terrigenic He cover a range of 70–75%.

A similar behavior can be observed for the Ne and Ar isotopes as shown in Fig. 6: both isotope ratios decrease with increasing tunnel depth. The decrease of the $^{36}Ar/^{40}Ar$ ratios can be explained by the accumulation of radiogenic ^{40}Ar produced by the decay of ^{40}K in the OPA pore waters (Rübel et al., 2002). For the decrease of the $^{20}Ne/^{22}Ne$ ratios, at least for the moment, we can only speculate that either the OPA pore water signature does not reflect the one of ASW (i.e., a $^{20}Ne/^{22}Ne$ ratio of about 9.78; Beyerle et al., 2000) or that some fractionation mechanism is affecting the Ne isotopes. In particular, two gas samples are characterized by Ne and Ar isotope ratios being significantly higher than the atmospheric air values (Fig. 6, open square). We hypothesize that these high Ne isotope ratios are produced by a fractionation process like, for instance, diffusion-controlled gas transport through the plug or the EDZ. Nonetheless, the observed trend in the isotope composition implies the presence of quite complex gas exchange processes that for the time being cannot be further constrained.

The elemental plot of the Ar/Kr ratios against the Ne/Kr ratios in Fig. 7 highlights again the gas exchange occurring between the OPA pore water and the gas phase in the bentonite pore space. The measured values (black dots) deviate significantly from the atmospheric air composition (open square) and follow a trend towards the elemental composition of OPA pore water (grey shaded area; Maineult et al., 2013). In the following we aim to investigate the observed elemental fractionation using two different approaches: 1) A binary mixing of OPA pore water gases with atmospheric air and 2) gas partitioning between OPA pore water and the free gas phase in the backfill pore space at solubility equilibrium. It should be noted that both approaches are intended to illustrate and estimate the gas dynamics on a conceptual level; they do not provide precise constraints on the gas exchange in the FE experiment.

Assuming a binary mixture of atmospheric air and an unfractionated pore water gas component (open circle in Fig. 7 being the average elemental ratios from Maineult et al., 2013) we can estimate the minimum shares of gas originating from the OPA at each sampling port to about 2–12% (average for all samples: (7 ± 2) %). It is possible to roughly assess the amount of pore water required to produce the observed elemental shift in the gas phase of the bentonite pore space using the measured Ne concentrations (Table 2) and the determined OPA pore water gas shares. The amount of Ne provided from the OPA pore

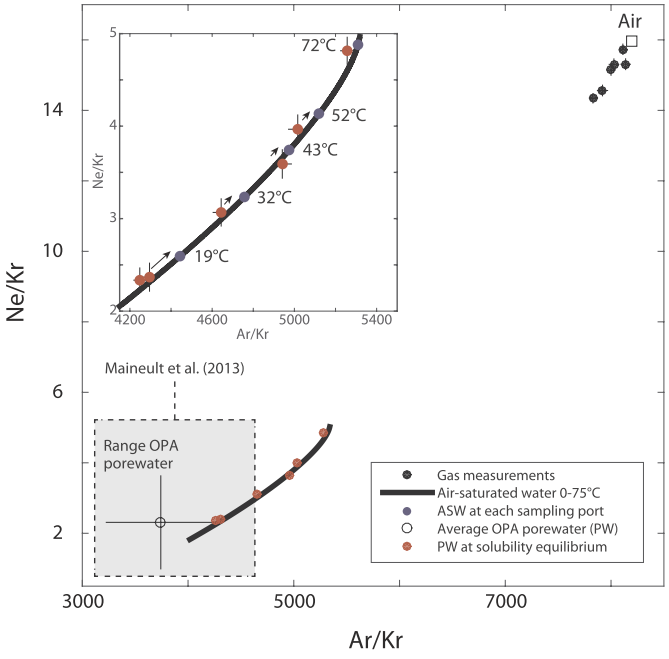

Fig. 7. Ar/Kr ratios against the Ne/Kr ratios. Black dots are the measured elemental ratios. The grey-shaded square indicates the value range from OPA pore water measurements performed by Maineult et al. (2013) and the open circle is the respective average. The gas in the bentonite pore space is characterized by an elemental signature that differs significantly from the one of atmospheric air (open square). The observed elemental fractionation could result from a binary mixing between atmospheric air and gas from the OPA pore water (open circle). However, if the measured free gas concentrations are converted into dissolved gas concentrations using the Henry coefficients for the local temperature conditions at each sampling port, the resulting concentrations (red dots) lie very close to the expected ASW values (thick black line). This suggests that part of the atmospheric air initially present in the bentonite pore space has been replaced by a significant share of gases from the surrounding OPA. In the inset plot the pore water elemental ratios (red dots) are compared with the expected ASW values (blue dots). The shift of the pore water signature towards "lower" temperatures compared to those for ASW suggests that the overall gas exchange is not yet at steady state. (For interpretation of the references to color in this figure legend, the reader is referred to the Web version of this article.)

water can be inferred by multiplying the determined Ne concentrations by the share of gas from the OPA and the volume of the bentonite pore space (~70 m^3 assuming a bulk bentonite volume of 160 m^3 and a porosity of 45%). The respective mass of water from where the total amount of Ne from the OPA should originate is then the Ne amount divided by the expected Ne concentration for ASW. From these simple calculations, at least 125–910 m^3 (average for all samples: V_{PW} = 500 m^3) of OPA pore water should have been involved in gas exchange.

The estimated pore water volumes are unexpectedly large but should be considered only as a zeroth-order estimation. Taking into account an OPA porosity (ϕ) of 16.4% (Gimmi et al., 2014) and a FE tunnel surface (A_{FE}) of about 280 m^2, the average depth of effective gas exchange ($\Delta x = V_{PW}/(\phi A_{FE})$) should be about 11 m. It should be noted that the characteristic length for diffusive transport of noble gases in bulk water $\Delta z = (2 \cdot D_{mol,i} \cdot t)^{1/2}$ (where $D_{mol,i}$ is the molecular diffusion coefficient of gas i = He, Ne, Ar, Kr, and Xe; t is the time between experiment closure and gas sampling) covers a range of 0.3–0.8 m. This clearly indicates that gas exchange in the FE experiment cannot be explained exclusively by diffusion of gases from the OPA pore water into the bentonite pore space through an interface being limited to the tunnel surface (as $\Delta z = \Delta x$ requires $A_{FE} \gg 280\ m^2$), i.e. purely diffusive transport in a pore water phase would require decades/centuries to produce the observed shift in the noble-gas elemental composition.

The physical partitioning between the liquid OPA pore water phase and the gas phase in the backfill pore space can be further investigated using the Henry coefficients $H_i(T,S)$ (i being the measured gas species Ne, Ar, Kr) for the specific temperature (T) and salinity (S) conditions prevailing at each gas sampling port (see e.g., Kipfer et al., 2002; Aeschbach-Hertig and Solomon, 2013; Brennwald et al., 2013). It is possible to infer the solubility equilibrium concentrations in the pore water ($C_{i,eq}$) from the measured partial pressures (p_i) according to Henry's law $p_i = H_i(T,S) \cdot C_{i,eq}$. The noble gas elemental signature for a water phase at solubility equilibrium with the gas phase in the FE experiment (Fig. 7, red dots) agrees well with the value range known for air-saturated water (ASW, thick black line). A slight deviation of the calculated equilibrium concentrations from ASW might result from the specific OPA pore water gas composition (grey shaded area in Fig. 7; Maineult et al., 2013).

In the inset plot of Fig. 7 the pore water elemental signatures at solubility equilibrium (red dots) are compared with those expected for ASW at each sampling port (blue dots). The temperatures given in the inset are the ones registered by the sensors close to each gas sampling port at the time of the sampling. A general shift of the pore water elemental ratios towards lower values with respect to the values for ASW suggests that the pore water signature might be indeed different compared to ASW. Although the original elemental and isotope signature of the OPA pore water cannot be fully constrained with the available empirical data (Maineult et al., 2013; Pearson et al., 2003), decreasing differences between the elemental composition of pore water at solubility equilibrium and the elemental composition of ASW with increasing temperatures make the case that gas partitioning is not yet at a steady state. This is reasonable, as the energy released by the three heaters in the FE experiment results in a continuous temperature increase in the bentonite/OPA and the mass transfer related to gas exchange is likely to be slower than energy transfer of the heating.

The general agreement of the calculated equilibrium concentrations (Fig. 7, red dots) with the expected ASW value range (Fig. 7, black solid line) makes the case that gas partitioning between liquid and gaseous phases in the FE experiment is effective. Hence, it seems that the initial atmospheric air signature (i.e., isotope and elemental composition) has been replaced to a significant extent with the OPA pore water signature.

The effective exchange of gases between the OPA pore water and the backfill pore space let us speculate that unconstrained geometrical factors foster the gas exchange within the FE experiment. A hypothesis could be that gases can access transport pathways not available for liquid phases 1) allowing faster gas transfer towards the backfill pore space and 2) providing additional surface for gas exchange within the OPA. From this point of view, the EDZ and EDZ-like features produced by mechanical disturbances of the OPA may play a major role in the overall gas transport. The formation of the EDZ has been shown to increase significantly the permeability of the host rock (Armand et al., 2008; Marschall et al., 2017) and the fracture network in the first meter of the EDZ was found to be well interconnected (Bossart et al., 2002). The boreholes drilled radially from the drift into the OPA as well as construction elements such as rock bolts (up to 7.5 m) and extensometers (up to 8 m) potentially also play a role in the diffusive transport of gases.

Gas exchange with the OPA could in part explain the disappearance of O_2 from the bentonite pore space, as illustrated by the published sensor data (up to ~1.2% per day; Giroud et al., 2018). Indeed, O_2 is totally absent in the OPA pore water and gas partitioning with a O_2-containing gas phase would result in O_2 transfer from this gas phase into the pore water phase. The highly reducing conditions in the OPA (similarly to the ones observed in Callovo-Oxfordian claystone; Vinsot et al., 2017b) could in principle sustain a high concentration gradient between the bentonite pore space and the OPA pore water fostering O_2 removal from the gas phase in the FE tunnel.

The Xe depth profile determined by conventional noble-gas

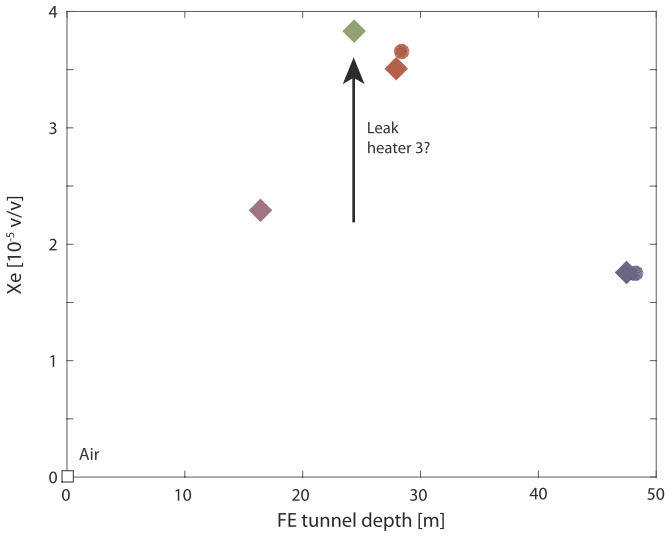

Fig. 8. Xe depth profile within the FE tunnel. A concentration maximum can be observed between heaters 2 and 3 (see Fig. 1). The measured Xe concentrations being three orders of magnitude higher than the atmospheric concentrations (open square, $8.7{\cdot}10^{-8}$ v/v) clearly indicate that Xe-spiked N_2 is leaking from one of the heaters (most likely heater 3 being involved in a fall incident prior to its emplacement; Aitemin, 2015).

measurements is shown in Fig. 8. The highest concentration of $3.8{\cdot}10^{-5}$ v/v is located between heater 2 and 3, as already suggested by the on-line gas monitoring (Section 3.1). This concentration is more than two orders of magnitude higher than the atmospheric air concentration ($8.7{\cdot}10^{-8}$ v/v). Such a huge Xe enrichment is clearly produced by gas leakage from one of the heaters containing Xe-spiked N_2 ($2{\cdot}10^{-3}$ v/v Xe) and explains why the quadrupole mass spectrometer of on-line gas monitoring system was able to detect differences between the various gas sampling ports. Despite the anthropogenic release of Xe being likely to hamper any detailed investigation of natural gas exchange processes in the FE experiment using this tracer (e.g., the Xe mass originating from the OPA of from the FE niche is negligibly small compared to the one from the heaters), further observation of the behavior of Xe might provide useful constraints on transport processes affecting other gas species. For instance, the detection of Xe enrichments in the region of the far-field instrumentation could allow estimation of the extent of the pathways accessible for gas transport provided by the EDZ.

4. Conclusions

The gas monitoring of the FE experiment at Mont Terri reveals complex processes affecting the gas species in the pore space of the bentonite used as tunnel backfilling and in the surrounding OPA.

Our results show that gas exchange with the surrounding OPA plays a significant role in the overall gas budget. The OPA pore waters seem to act both as source (e.g., He, Ar, CH_4, CO_2) and sink (e.g., O_2) for atmospheric and terrigenic gases. Gas exchange with the OPA pore waters is expected and it can explain in part the O_2 partial pressure decrease detected by O_2 sensors during the initial phase of the experiment. Oxygen removal (and the respective total pressure drop) is likely to have induced the inflow of atmospheric air from the FE niche into the bentonite pore space immediately after closure of the FE experiment.

Additional data are needed to better understand the processes controlling the CO_2 concentrations in the bentonite backfill. In particular, stable isotopes analyzed in gas samples may provide a better insight on the influence of microbial activity on the behavior of CO_2.

Although H_2 has been detected, suggesting the onset of anaerobic steel corrosion, the highest H_2 partial pressure was only 0.6 mbar (0.06%). CH_4 showed a maximum enrichment of 1.3 mbar (0.1%).

Based on the insights provided by the on-line gas monitoring of the FE experiment, it is difficult to fully understand on a conceptual level the gas dynamics during the early stages and even at present. The instrumentation of the FE tunnel (e.g., boreholes with multi-packer systems, several hundred sensors with the respective wiring) could be in part responsible for experimental artifacts in terms of gas transport (e.g., preferential pathways), that cannot be clearly identified with the limited amount of data available. Also, the impact of EDZ and EDZ-like structures cannot be further constrained with the available data. The ongoing gas monitoring in the FE experiment, together with the acquisition and interpretation of thermo-hydro-mechanical data over several more years, should improve our understanding of these structures in the future. Additionally, the use of tracer gases between the backfill and the far-field may also provide useful information.

Acknowledgements

We would like to thank the Special Issue Editor Dr. Cathelineau and two anonymous reviewers for their valuable comments on the manuscript. The FE experiment is part of the Mont Terri Project, which is operated by Swisstopo. The FE-G experiment benefited from financial support from Andra (France), Nagra (Switzerland), and NWMO (Canada). The authors wish to thank the FE implementation team for making this unique experiment possible. Edith Horstmann was supported by the Swiss National Science Foundation (SNF grant no. 20021_162447).

References

Aeschbach-Hertig, W., Solomon, D.K., 2013. Noble gas thermometry in groundwater hydrology. In: Burnard, P., Hoefs, J. (Eds.), The Noble Gases as Geochemical Tracers. Springer, Berlin, Heidelberg, pp. 81–122. https://doi.org/10.1007/978-3-642-28836-4_5. Advances in Isotope Geochemistry.

Aitemin, 2015. FE-Experiment – Heater 3: Status after the Fall Incident, Remedial Actions Carried Out and Final Status. Technical Report TN 2015-41. Mont Terri Project.

Armand, G., Blümling, P., Frank, E., Frieg, B., Löw, S., Mayor, J.C., Volckaert, G., 2008. EDZ (including self-sealing) experiments. In: Bossart, P., Thury, M. (Eds.), Mont Terri Rock Laboratory – Project, Programme 1996 to 2007 and Results. Federal Office of Topography (Swisstopo). Reports of the Swiss Geological Survey, pp. 133–144.

Baur, H., 1980. Numerische Simulation und praktische Erprobung einer rotations-symmetrischen Ionenquelle für Gasmassenspektrometer. Ph.D. thesis. ETH Zürich, Switzerland.

Beyerle, U., Aeschbach-Hertig, W., Imboden, D.M., Baur, H., Graf, T., Kipfer, R., 2000. A mass spectrometric system for the analysis of noble gases and tritium from water samples. Environ. Sci. Technol. 34, 2042–2050. https://doi.org/10.1021/es990840h.

Bossart, P., Meier, P.M., Moeri, A., Trick, T., Mayor, J.C., 2002. Geological and hydraulic characterisation of the excavation disturbed zone in the Opalinus clay of the Mont Terri rock laboratory. Eng. Geol. 66, 19–38. https://doi.org/10.1016/S0013-7952(01)00140-5.

Brennwald, M.S., Schmidt, M., Oser, J., Kipfer, R., 2016. A portable and autonomous mass spectrometric system for on-site environmental gas analysis. Environ. Sci. Technol. 50, 13455–13463. https://doi.org/10.1021/acs.est.6b03669.

Brennwald, M.S., Vogel, N., Scheidegger, Y., Tomonaga, Y., Livingstone, D.M., Kipfer, R., 2013. Noble gases as environmental tracers in sediment porewaters and in stalagmite fluid inclusions. In: Burnard, P., Hoefs, J. (Eds.), The Noble Gases as Geochemical Tracers. Springer, Berlin, Heidelberg, pp. 123–153. https://doi.org/10.1007/978-3-642-28836-4_6. Advances in Isotope Geochemistry.

Diomidis, N., Cloet, V., Leupin, O., Marschall, P., Poller, A., Stein, M., 2016. Production, Consumption and Transport of Gases in Deep Geological Repositories According to the Swiss Disposal Concept. Technical Report NTB 16-03. Nagra, Wettingen, Switzerland.

Gimmi, T., Leupin, O.X., Eikenberg, J., Glaus, M.A., Loon, L.R.V., Waber, H.N., Wersin, P., Wang, H.A., Grolimund, D., Borca, C.N., Dewonck, S., Wittebroodt, C., 2014. Anisotropic diffusion at the field scale in a 4-year multi-tracer diffusion and retention experiment – I: insights from the experimental data. Geochim. Cosmochim. Acta 125, 373–393. https://doi.org/10.1016/j.gca.2013.10.014.

Giroud, N., Tomonaga, Y., Wersin, P., Briggs, S., King, F., Vogt, T., Diomidis, N., 2018. On the fate of oxygen in a spent fuel emplacement drift in Opalinus Clay. Appl. Geochem. 97, 270–278. https://doi.org/10.1016/j.apgeochem.2018.08.011.

Kipfer, R., Aeschbach-Hertig, W., Peeters, F., Stute, M., 2002. Noble gases in lakes and ground waters. In: Porcelli, D., Ballentine, C., Wieler, R. (Eds.), Noble Gases in Geochemistry and Cosmochemistry. Mineralogical Society of America, Geochemical Society. Volume 47 of Reviews in Mineralogy and Geochemistry, pp. 615–700. https://doi.org/10.2138/rmg.2002.47.14.

Lee, J.Y., Marti, K., Severinghaus, J.P., Kawamura, K., Yoo, H.S., Lee, J.B., Kim, J.S.,

2006. A redetermination of the isotopic abundances of atmospheric Ar. Geochim. Cosmochim. Acta 70, 4507–4512.
Liu, J.F., Song, S.B., Ni, H.Y., Cao, X.L., Pu, H., Mao, X.B., Skoczylas, F., 2018a. Research on gas migration properties in a saturated bentonite/sand mixture under flexible boundary conditions. Soils Found. 58, 97–109.
Liu, J.F., Wu, Y., Cai, C.Z., Ni, H.Y., Cao, X.L., Pu, H., Song, S.B., Pu, S.Y., Skoczylas, F., 2018b. Investigation into water retention and gas permeability of Opalinus Clay. Environ. Earth Sci. 77, 213.
Maineult, A., Thomas, B., Nussbaum, C., Wieczorek, K., Gibert, D., Lavielle, B., Kergosien, B., Nicollin, F., Mahiouz, K., Lesparre, N., 2013. Anomalies of noble gases and self-potential associated with fractures and fluid dynamics in a horizontal borehole, Mont Terri Underground Rock Laboratory. Eng. Geol. 156, 46–57. https://doi.org/10.1016/j.enggeo.2013.01.010.
Mamyrin, B.A., Tolstikhin, I.N., 1984. Helium Isotopes in Nature. Volume 3 of Developments in Geochemistry, 1 ed. Elsevier, Amsterdam, Oxford, New York, Tokyo.
Marschall, P., Giger, S., De La Vassière, R., Shao, H., Leung, H., Nussbaum, C., Trick, T., Lanyon, B., Senger, R., Lisjak, A., Alcoleam, A., 2017. Hydro-mechanical evolution of the EDZ as transport path for radionuclides and gas: insights from the Mont Terri rock laboratory (Switzerland). Swiss J. Geosci. 110, 173–194. https://doi.org/10.1007/s00015-016-0246-z.
Mazurek, M., Alt-Epping, P., Bath, A., Gimmi, T., Waber, H.N., Buschaert, S., Cannière, P.D., Craen, M.D., Gautschi, A., Savoye, S., Vinsot, A., Wemaere, I., Wouters, L., 2011. Natural tracer profiles across argillaceous formations. Appl. Geochem. 26, 1035–1064. https://doi.org/10.1016/j.apgeochem.2011.03.124.
Müller, H.R., Garitte, B., Vogt, T., Köhler, S., Sakaki, T., Weber, H., Spillmann, T., Hertrich, M., Becker, J.K., Giroud, N., Cloet, V., Diomidis, N., Vietor, T., 2017. Implementation of the full-scale emplacement (FE) experiment at the Mont Terri rock laboratory. Swiss J. Geosci. 110, 287–306. https://doi.org/10.1007/s00015-016-0251-2.
Nagra, 2010. Beurteilung der geologischen Unterlagen für die provisorischen Sicherheitsanalysen in SGT Etappe 2. Klärung der Notwendigkeit ergänzender geologischer Untersuchungen. Technical Report NTB 10-01. Nagra, Wettingen, Switzerland.
Ozima, M., Podosek, F.A., 1983. Noble Gas Geochemistry. Cambridge University Press, Cambridge, London, New York.
Pearson, F., Tournassat, C., Gaucher, E.C., 2011. Biogeochemical processes in a clay formation in situ experiment: Part E – equilibrium controls on chemistry of pore water from the Opalinus Clay, Mont Terri Underground Research Laboratory, Switzerland. Appl. Geochem. 26, 990–1008. https://doi.org/10.1016/j.apgeochem.2011.03.008.
Pearson, F.J., Arcos, D., Bath, A., Boisson, J.Y., Fernndez, A.M., Gäbler, H.E., Gaucher, E., Gautschi, A., Griffault, L., Hernán, P., Waber, H.N., 2003. Mont Terri Project – Geochemistry of Water in the Opalinus Clay Formation at the Mont Terri Rock Laboratory. Reports of the Federal Office for Water and Geology (FOWG), Geology Series No. 5. Federal Office of Topography (swisstopo).
Rösli, U., Gisiger, J., 2016. Mont Terri FE-B Experiment – Installation of Tunnel Wall, Bentonite and In-situ Gas Equipment Instrumentation for Long Term THM Monitoring (Phase 3). Technical Report TN 2014-52. Solexperts AG, Mönchaltdorf, Switzerland.
Rösli, U., Lettry, Y., 2016. Mont Terri FE-G Experiment Phase 21 – Delivery and Installation of Gas Module. Technical Report TN 2016-68. Solexperts AG, Mönchaltdorf, Switzerland.
Rübel, A.P., Sonntag, C., Lippmann, J., Pearson, F.J., Gautschi, A., 2002. Solute transport in formations of very low permeability: profiles of stable isotope and dissolved noble gas contents of pore water in the Opalinus Clay, Mont Terri, Switzerland. Geochim. Cosmochim. Acta 66, 1311–1321. https://doi.org/10.1016/S0016-7037(01)00859-6.
Sano, Y., Marty, B., Burnard, P., 2013. Noble gases in the atmosphere. In: Burnard, P., Hoefs, J. (Eds.), The Noble Gases as Geochemical Tracers. Springer, Berlin, Heidelberg, pp. 17–31. https://doi.org/10.1007/978-3-642-28836-4_2. Advances in Isotope Geochemistry.
Tomonaga, Y., Brennwald, M., Kipfer, R., 2011. An improved method for the analysis of dissolved noble gases in the pore water of unconsolidated sediments. Limnol. Oceanogr. Methods 9, 42–49. https://doi.org/10.4319/lom.2011.9.42.
Tomonaga, Y., Marzocchi, R., Pera, S., Pfeifer, H.R., Kipfer, R., Decrouy, L., Vennemann, T., 2017. Using noble-gas and stable-isotope data to determine groundwater origin and flow regimes: Application to the Ceneri Base Tunnel (Switzerland). J. Hydrol. 545, 395–409. https://doi.org/10.1016/j.jhydrol.2016.11.043.
Tyroller, L., Tomonaga, Y., Brennwald, M.S., Ndayisaba, C., Naeher, S., Schubert, C., North, R.P., Kipfer, R., 2016. Improved method for the quantification of methane concentrations in unconsolidated lake sediments. Environ. Sci. Technol. 50, 7047–7055. https://doi.org/10.1021/acs.est.5b05292.
Vinsot, A., Appelo, C.A.J., Lundy, M., Wechner, S., Cailteau-Fischbach, C., de Donato, P., Pironon, J., Lettry, Y., Lerouge, C., De Cannière, P., 2017a. Natural gas extraction and artificial gas injection experiments in Opalinus Clay, Mont Terri rock laboratory (Switzerland). Swiss J. Geosci. 110, 375–390. https://doi.org/10.1007/s00015-016-0244-1.
Vinsot, A., Appelo, C.A.J., Lundy, M., Wechner, S., Lettry, Y., Lerouge, C., Fernández, A.M., Labat, M., Tournassat, C., De Canniere, P., Schwyn, B., Mckelvie, J., Dewonck, S., Bossart, P., Delay, J., 2014. In situ diffusion test of hydrogen gas in the opalinus clay. Geol. Soc., Lond., Spec. Publ. 400, 563–578. https://doi.org/10.1144/SP400.12.
Vinsot, A., Lundy, M., Linard, Y., 2017b. O_2 consumption and CO_2 production at Callovian-Oxfordian rock surfaces. Proc. Earth. Plan. Sc. 17, 562–565. https://doi.org/10.1016/j.proeps.2016.12.142.
Waber, H.N., Rufer, D., 2017. Porewater Geochemistry, Method Comparison and Opalinus Clay – Passwang Formation Interface Study at the Mont Terri URL. Technical Report NWMO-TR-2017-10. Nuclear Waste Management Organization, Toronto, Canada.